nature geoscience

ARTICLES

https://doi.org/10.1038/s41561-018-0166-9

Highland cropland expansion and forest loss in Southeast Asia in the twenty-first century

Zhenzhong Zeng[1*], Lyndon Estes[2], Alan D. Ziegler[3], Anping Chen[4], Timothy Searchinger[5], Fangyuan Hua[6], Kaiyu Guan[7], Attachai Jintrawet[8] and Eric F. Wood[1]

Southeast Asia is a hotspot of tropical deforestation for agriculture. Most of the deforestation is thought to occur in lowland forests, whereas the region's mountainous highlands undergo very limited deforestation. However, regional reports of cropland expansion in some highland areas suggest that this assumption is inaccurate. Here we investigate patterns of forest change and cropland expansion in the region for the twenty-first century, based on multiple streams of state-of-the-art satellite imagery. We find large increases in cultivated areas that have not been documented or projected. Many of these cultivated areas have evolved from forests that vary in health and status, including primary and protected forests, or from recovering lands that were on a trajectory to become secondary forests. These areas all have different biophysical features than croplands. We estimate that an area of 82 billion m² has been developed into croplands in the Southeast Asian highlands. Some portion of this land-use change is probably attributable to agricultural intensification on formerly swidden agriculture lands; however, a substantial proportion is from new forest loss. Our findings are in marked contrast with projections of land-cover trends that currently inform the prediction of future climate change, terrestrial carbon storage, biomass, biodiversity, and land degradation.

Land-cover change, particularly tropical forest conversion, is an important driver of the dynamics of the Earth system, having pronounced effects on climate, food, energy and ecological systems[1–8]. In recent decades, some of the fastest rates of tropical forest loss have occurred in Southeast Asia (SEA)[9–12]. The abrupt loss of carbon- and species-rich forests may have profound socio-economic and environmental impacts, including modification of regional to global climate[1,2,7], changes in water balances at various scales, loss of globally unique biodiversity[6,8] and disruption to other important environmental services[13,14]. The nature of these impacts can vary depending on the spatial distribution and intensity of forest removal, and whether forest removal is permanent (aka deforestation) and/or involves fire, logging or intense cultivation[2,5,7,15]. Resolving the extent and drivers of recent forest loss patterns in SEA is therefore important for understanding its negative impacts on environmental systems in the future.

Earlier work suggests that agricultural expansion in the lowlands has been the major driver of forest loss in SEA[6,8]. Agricultural expansion in the highlands are rarely observed, except for tree-based plantations (mainly rubber) in mainland SEA[16–19]. For example, recent studies[16,17] projected an expansion of rubber plantations into sub-optimal areas (including the highlands) where higher altitudes, steeper slopes, and low temperatures may limit yields. The generally accepted view of future land-cover evolution in the highlands of SEA aligns with the expectation of a persistence of various states of forest and tree-dominated land cover, including tree plantations, but little conversion to croplands[16–19]. Aligning with the general view that cropland expansion in highland areas is not economically feasible, the United Nations Food and Agriculture Organization (FAO) has projected little to no net expansion of croplands in the region[20].

These predictions and their foundational assumptions underlie various environmental impact assessments, principally the modelling analyses of the Intergovernmental Panel on Climate Change (IPCC) that project global and regional changes in climate[1,2]. However, recent studies conducted in local settings suggest that substantial forest losses in some highland areas (such as the Nan province, Thailand) were caused by the expansion of croplands[21,22] (see Fig. 1). By articulating land-cover changes that differ from the accepted projections in the region, these particular studies[21,22] motivated us to investigate whether forest loss in the highlands has become more prominent because of cropland expansion. The geographically diverse highlands are ecologically fragile areas that are refuges of biodiversity and water towers for lowland population centres[23,24]. In this setting, highland agriculture imposes a distinct and pronounced set of impacts. For example, the expansion of steep-slope cropping exacerbates soil erosion, increases landslide risk and alters stream flow[21,23,24]. In-situ land degradation associated with stationary cropping leads to progressive yield declines that force farmers to increase fertilizer and other chemical inputs[21,22]. Accelerated erosion and runoff of agricultural pollutants may degrade water quality, and increased sediment loads may lead to rapid filling in downstream dams and retention structures. From a climate perspective, topographical features (slope, aspect, elevation) interact in different ways with vegetation types to impact cloud formation, precipitation and mesoscale turbulent heat fluxes and circulation[25,26]. Large-scale expansion of croplands into the topographically complex, predominantly forested highlands may therefore have substantial, but hard to predict, effects on local to regional climate, including the monsoon[25–27].

[1]Department of Civil and Environmental Engineering, Princeton University, Princeton, NJ, USA. [2]Graduate School of Geography, Clark University, Worcester, MA, USA. [3]Geography Department, National University of Singapore, Singapore, Singapore. [4]Forestry and Natural Resources, Purdue University, West Lafayette, IN, USA. [5]Woodrow Wilson School, Princeton University, Princeton, NJ, USA. [6]Department of Zoology, University of Cambridge, Cambridge, UK. [7]Natural Resources and Environmental Sciences, University of Illinois at Urbana Champaign, Urbana, IL, USA. [8]Department of Plant and Soil Sciences, Faculty of Agriculture, Chiang Mai University, Chiang Mai, Thailand. *e-mail: zzeng@princeton.edu

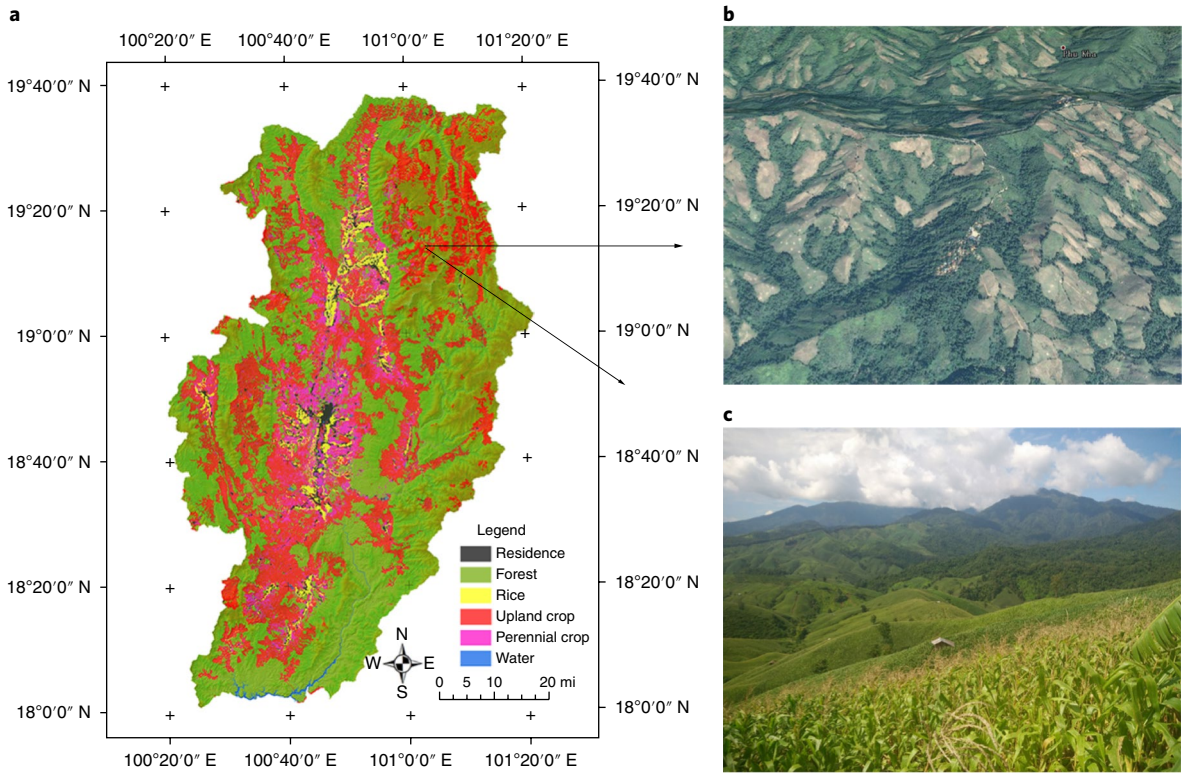

Fig. 1 | Cropland expansion along topographical frontiers in the twenty-first century in Nan province, Thailand. a, The RapidEye (5 m resolution) satellite-observed land-cover maps in 2017, separating residence, forest, rice, upland crop, perennial crop and water. Nan is a hilly and mountainous province located in northern Thailand. The data were produced by the Geo-Informatics and Space Technology Development Agency (GISTDA), obtained from KASIKORN Foundation in Thailand. **b**, An aerial view of formerly forested land converted to croplands in the highlands, obtained from Google Earth (CNES/Airbus, image date: 2 February 2014). **c**, Photograph of general area of **b** on 24 August 2016.

A novel approach to uncover land-cover change

In this study, we conducted a comprehensive assessment of the cropland expansion patterns in SEA's forest frontiers during the twenty-first century, for which we (1) distinguish between highland and lowland forest loss, and (2) determine the extent to which recent losses were driven by cropland expansion. Our analysis is based on the high-resolution global maps of twenty-first-century forest cover (hereafter referred to as HANSEN[28]), which delineate forest loss and gain patterns since 2000 (see Methods for details). First, we define cropland as areas that grow commercial or subsistence products including annual (for example, rice, corn) and some perennial (such as coffee, tea) crops. We recognize that many taller perennial (tree) crops (for example, rubber, oil palm and various fruit trees) are often not distinguished from natural forests by vegetation maps that separate forested from non-forested land using thresholds based on tree cover[28–30]. Under such approaches, forest loss is defined as the removal or mortality of tree cover; and forest gain as the establishment of tree cover from a non-tree state. Here we adopt these definitions, as well as the associated definition of trees being any vegetation taller than 5 m in height[28]. In this case, we count tree crops that meet this height criterion as forests, rather than croplands[30], as we focus on structural changes in vegetation that may significantly impact climate and other environmental processes. Our treatment of tree crops is consistent with land-cover classifications used by climate models, in which tree crops are classified as the same 'plant functional type' as forests because of the similarity of their biophysical and carbon sequestration characteristics. We also define net forest loss areas (NFLAs) as the pixels ($30 \times 30\,m^2$) where HANSEN product indicates only forest loss and no gain during any year of the twenty-first century.

Second, we apply a stratified approach following Olofsson and colleagues[31] for accuracy assessment and area estimation of HANSEN-derived NFLAs. We use high-resolution satellite imagery from around 2000 and 2014 to interpret forest cover change in 1,500 lowland and 2,500 highland sample pixels that were selected from NFLAs at random, as well as 500 lowland and 500 highland sample pixels randomly selected from non-NFLAs (Supplementary Data 1–4). In SEA, the overall, user's and producer's accuracies of HANSEN-derived NFLAs are 98.4%, 93.2% and 81.2%, respectively (for further assessment see Methods). Third, we determined the fate of forest loss in NFLAs using high-quality, cloud-free, high-resolution (≤5 m) Planet Lab (for example, from the Doves and RapidEye satellites) and Google Earth (for example, from the IKONOS, QuickBird, and Pleiades satellites) imagery that allows interpretation of the recent land cover (approximately 2014) in the 1,500 lowland and 2,500 highland sample pixels (see Methods).

Finally, to highlight the uncertainties in current knowledge of forest change/agricultural expansion patterns in this region—which could affect assessments of the impacts of land-cover change—we evaluated the patterns in several of the most up-to-date land-cover datasets, including the global land-cover reconstructions used in the transient climate simulations that inform the current and next generation IPCC Assessment Reports (IPCC AR5 and AR6; LCMIP5_RCP26, LCMIP5_RCP45, LCMIP5_RCP60, LCMIP5_RCP85 (ref. [1]), and LCMIP6 (ref. [32]); Supplementary Table 1). We also evaluated several datasets that allow a moderate- to high-resolution determination of recent land-cover change, namely several state-of-the-art global satellite-based land-cover products: MCD12Q (ref. [33]), ESACCI (ref. [34]) and GlobeLand30 (ref. [35] (Supplementary Table 2 and Methods).

Rapid forest loss in SEA during the twenty-first century

Figure 2a shows the spatial patterns of HANSEN-derived NFLAs from 2000 to 2014, aggregated to 0.25° cells (67.8–77.3 $\times 10^7$ m^2 in each cell). Different forest loss patterns occurred in highland areas, defined here as lands above 300 m elevation (dotted areas in Fig. 2a, a total of 192 $\times 10^{10}$ m^2) following Scott[36], versus the lowland areas below that elevation (non-dotted areas in Fig. 2a, comprising 250 $\times 10^{10}$ m^2). Extensive highland forest loss occurred in mainland SEA, whereas forest loss in maritime SEA was primarily confined to the lowlands, although several small regions of highland forest loss are also evident (Fig. 2a). We find that the substantial lowland forest loss in Indonesia in the late twentieth century reported by Curran et al.[9] has continued into the twenty-first century. Importantly, we also find that the highest median forest loss occurred in montane mainland SEA (2.51 $\times 10^7$ m^2 per cell; hereafter all area estimates are based on our reference sample following earlier studies[31,37]; Fig. 2b). The total forest loss in SEA is 29.3 $\times 10^{10}$ m^2 (26.3–32.3, 95% confidence interval) during the period 2000 to 2014, accounting for 11.3% of the total forest cover at the beginning of the twenty-first century (Supplementary Fig. 1).

Using our HANSEN-derived, sample-based estimates as a baseline, we conclude that rapid forest loss in SEA during the twenty-first century is generally underestimated in the land-cover change scenarios used in IPCC AR5 (Representative Concentration Pathways, RCP2.6, RCP4.5, RCP6.0 and RCP8.5, black bars in Fig. 2c). The AR5 climate simulations based on these scenarios are therefore likely to underestimate the effects of carbon emissions and other biophysical feedbacks caused by land-cover change in SEA. Forest loss rates calculated from the recent scenario prepared for IPCC AR6 simulations, which draw on FAO statistics, are closer to our estimates, yet still underestimate twenty-first-century forest loss in SEA by 36% (18.7 $\times 10^{10}$ m^2, green bar in Fig. 2c). Despite their use of direct

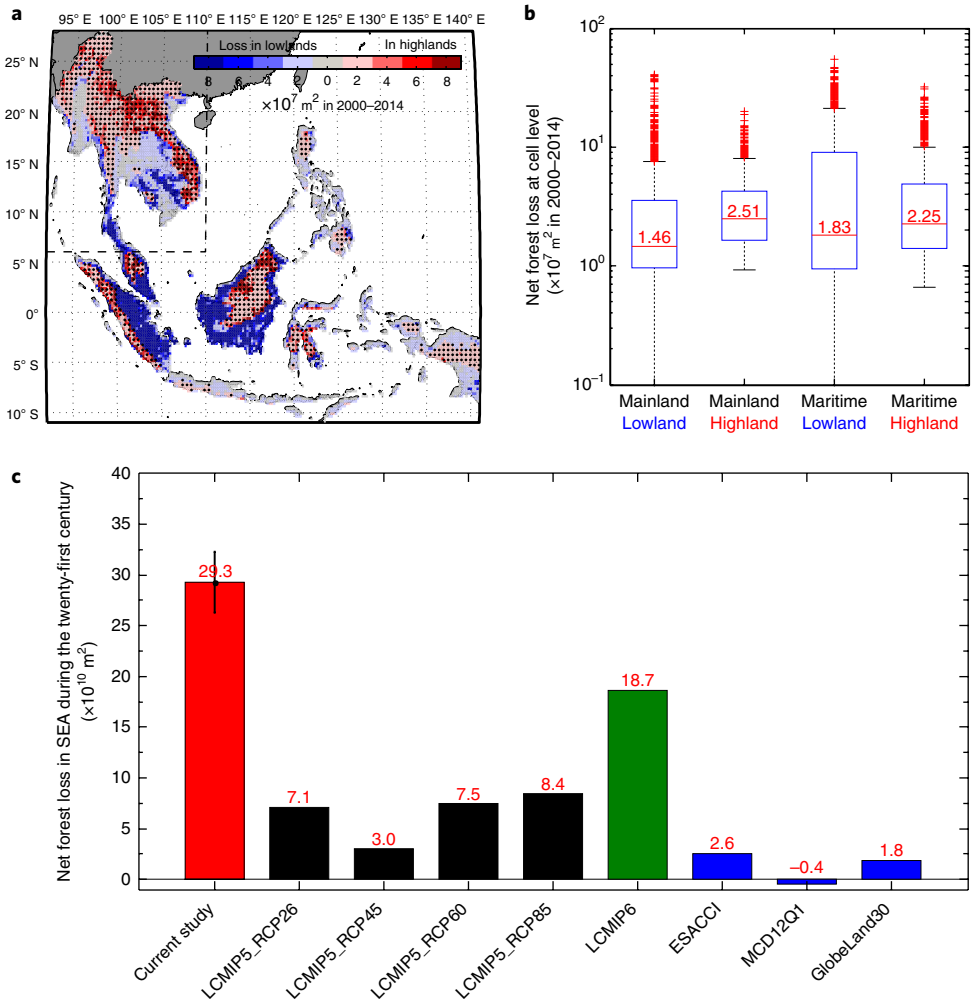

Fig. 2 | Spatial pattern and magnitude of net forest loss in SEA during the early twenty-first century. a, The areas experiencing net forest loss during 2000–2014 (colour scale; red indicates forest loss in highlands and blue in lowlands), based on HANSEN product by aggregating pixels showing only forest loss and no period of gain in each 0.25° cell. Stippling represents highland SEA. Black dashed lines separate mainland SEA from maritime SEA. **b**, Statistics of net forest loss at cell level (sample-based area estimates following earlier studies[31,37]) in the lowlands and highlands of mainland and maritime SEA. Note that for the estimates in highlands (lowlands), the error matrix of sample counts in highlands (lowlands) were applied. The central line (and value) is the median; box boundaries represent the 25th and 75th percentiles; whiskers represent 99.3% coverage of the data; outliers are plotted individually (crosses). **c**, Magnitude of net forest loss in SEA during the early twenty-first century. The sample-based estimate of this study (red bar) integrates HANSAN NFLAs with our reference sample following earlier studies[31,37] (2000–2014; the error bar shows the 95% confidence interval). The black bars are estimates from the land-cover change scenarios used for IPCC AR5 (RCP2.6, RCP4.5, RCP6.0 and RCP8.5; 2000–2014). The green bar is an estimate from data on land-cover change used for IPCC AR6 (2000–2014). The blue bars are estimates from the satellite-based products of land-cover change (ESACCI, 2000–2010; MCD12Q1, 2001–2011; GlobeLand30, 2000–2010).

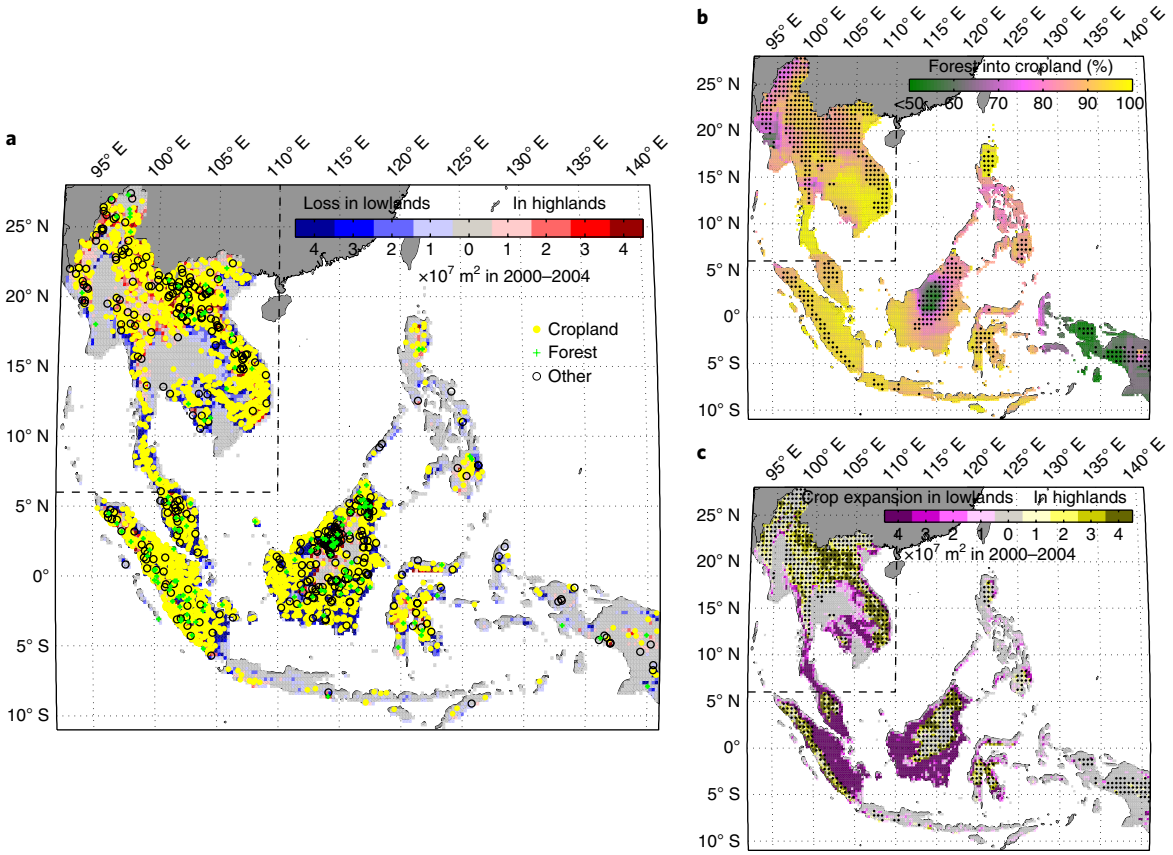

Fig. 3 | Spatial pattern of cropland expansion in SEA during the early twenty-first century. a, Visual interpretation of high-resolution (≤5 m) satellite imagery (around 2014) from the Planet Lab and Google Earth for 1,500 lowland and 2,500 highland sites randomly sampled from pixels where HANSEN product identified forest loss but no gain during 2000–2014. The background shading (colour scale) shows the NFLAs derived from Fig. 2a. Symbols indicate the sampled sites having changed into cropland, forest (indicating an error in HANSEN) or other (for example, urban, village, water, roads) land use. **b**, Percentage of forest loss into cropland in each 0.25° cell (δ_{crop}^{forest}) using all of the sampled sites within the 3°×3° window centred on the cell. **c**, Spatial patterns of twenty-first-century cropland expansion in SEA calculated by multiplying the areas of forest loss with no gain (Fig. 2a) by δ_{crop}^{forest} in each 0.25° cell (see **b**).

observations and rigorous classification methods, the satellite-based land-cover products (ESACCI, MCD12Q1 and GlobeLand30) fail to detect most of this forest loss (blue bars in Fig. 2c).

Inconsistent definitions of forest could be one reason for the difference in forest loss rates between the sample-based estimate (this study) and various land-cover products (Fig. 2c). Again, because the forest definition used by HANSEN product and adopted here is based solely on the presence of tree cover, we counted the expansion of tree crops taller than 5 m as forest gain[28,30]. Here we excluded all types of forest gain (including regrowth and plantation) from NFLAs (Supplementary Fig. 2). However, if all tree-crop expansion[16–19] is classified as forest loss rather than forest gain (by other definitions of forest), the loss of 'natural' forest (regardless of health/status) in SEA during the twenty-first century would be even greater. Another reason for the discrepancies could be that swidden fields are not a land-cover type that is recognized in global land-cover products, whereas yearly and aggregated forest gain and loss due to land-use dynamics in areas where swidden cultivation occurs are detectable from high-resolution Earth observation imagery (such as the Landsat imagery used in HANSEN). However, to minimize the effects of both tree-crop expansion and traditional land-use dynamics in swidden fields on our estimate of forest loss, we have excluded pixels that show both forest loss and gain within the study period. Thus, for swidden fields with rotations occurring during 2000 to 2014, there are co-occurrences of both forest loss and gain in the same pixels during the period; these areas have therefore been excluded from NFLAs in our analysis. It should be noted that our estimates include new swidden fields (probably opened from secondary forest rather than primary forest), as well as swidden fields that have been converted to continuous annual cropping systems[38–40].

Cropland expansion drives rapid forest loss

Using visual interpretation of high-resolution satellite imagery from the Planet Lab and Google Earth in 1,500 lowland and 2,500 highland pixels randomly selected from NFLAs (Supplementary Data 1 and 2), we found that cropland expansion was responsible for 94% and 88% of the recent (up to 2014) total forest loss in the lowlands (20.0 $\times10^{10}$ m^2, range 19.8–20.3 $\times10^{10}$ m^2) and highlands (9.3 $\times10^{10}$ m^2, range 9.1–9.5 $\times10^{10}$ m^2), respectively (Fig. 3a, Supplementary Fig. 3). That is to say, a total of about 27.0 $\times10^{10}$ m^2 of new croplands have been converted from forest in SEA, including approximately 8.2 $\times10^{10}$ m^2 in highland areas.

We used these sample pixels to map the percentage of forest conversion to cropland in 3°×3° moving windows (Fig. 3b), and mapped the spatial patterns of twenty-first-century cropland expansion in SEA (Fig. 3c; Methods). The combined estimate of cropland expansion and forest cover change (Fig. 4a; see Methods) differs substantially from those shown by all four land-cover products used for IPCC AR5 (mainly representing land-cover projections between 2006 and 2014), which show much more uniform spatial patterns of cropland expansion and forest loss (Fig. 4b–e). The projections for IPCC AR5 therefore underestimate the magnitude of highland

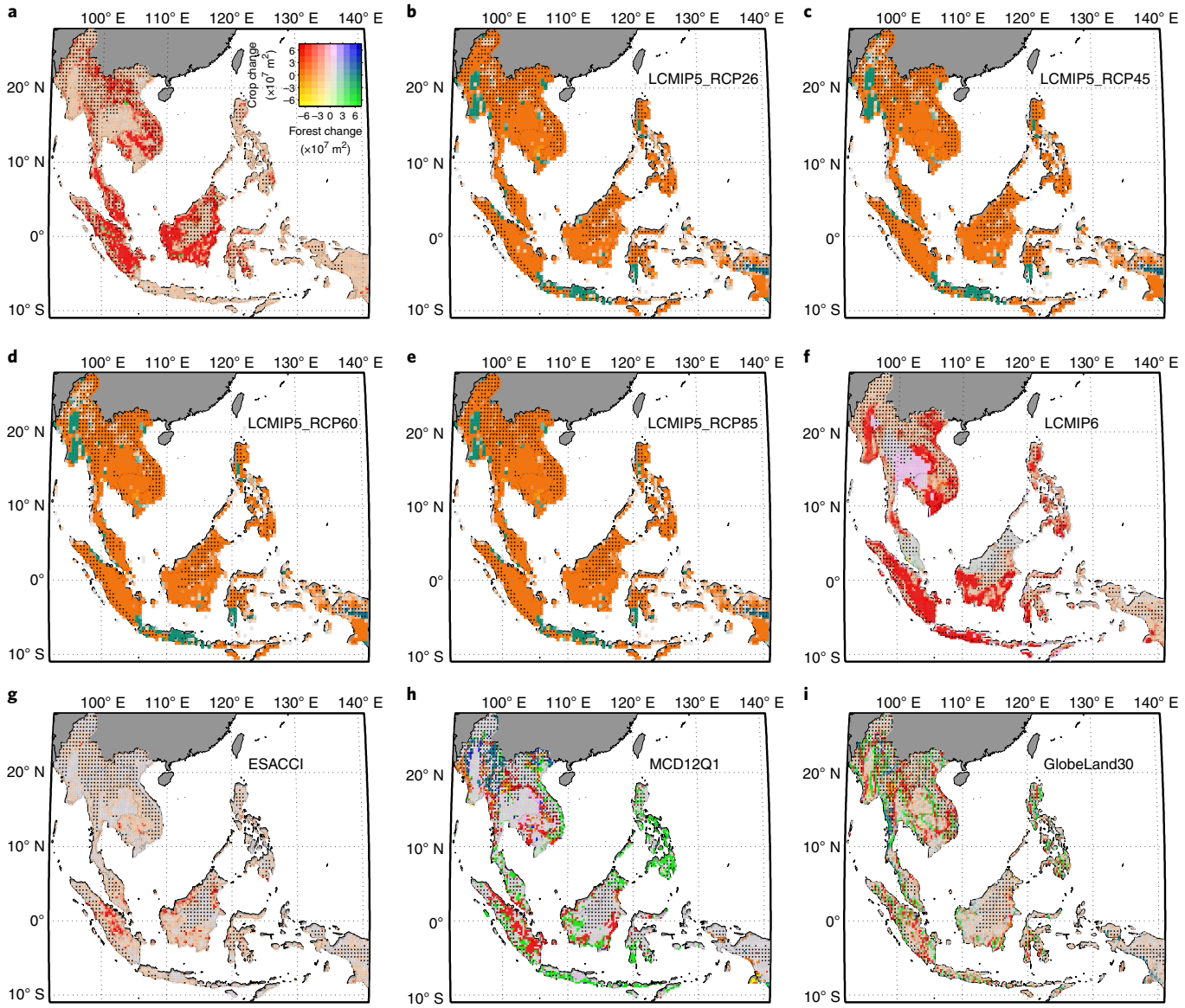

Fig. 4 | Evaluation on the spatial pattern of cropland expansion and forest change in SEA during the early twenty-first century for various products. a, Pattern based on the HANSEN-observed forest cover change (2000–2014) and the imputed cropland expansion (this study). **b**–**e**, Changes in crop and forest cover between 2000 and 2014 from data on global land cover used for AR5 RCP2.6 (**b**), RCP4.5 (**c**), RCP6.0 (**d**) and RCP8.5 (**e**). **f**, Changes in crop and forest cover between 2000 and 2014 based land-cover data used for IPCC AR6. **g**, Changes in crop and forest cover between 2000 and 2010 from the ESACCI satellite-based global product for land cover change. **h**, Changes in crop and forest cover between 2001 and 2011 from the MCD12Q1 satellite-based global product for land cover change. **i**, Changes in crop and forest cover between 2000 and 2010 from the GlobeLand30 satellite-based global product for land cover change. Stippling indicates highland SEA.

cropland expansion that has occurred in much of mainland SEA (Myanmar, Thailand, Laos and Vietnam, for example), while overestimating it in maritime SEA. The newer land-cover product used for IPCC AR6 (Fig. 4f) shows land-cover patterns that are closer to those in our HANSEN-based analysis, but still largely misses forest loss driven by cropland expansion in the highlands of mainland SEA.

Unlike the aforementioned land-cover reconstructions, the satellite-derived land-cover products have a much higher resolution and do not rely on national-scale agricultural statistics. Despite their finer grain, maps derived from these products (ESACCI, MCD12Q1 and GlobeLand30) showed even larger deviations from the patterns revealed by our HANSEN-based analysis, as well as substantial disagreement amongst themselves (Fig. 4g–i). Although these datasets capture the strong correlation between forest loss and cropland expansion revealed by our analysis (Supplementary Fig. 4), they underestimate forest loss because of problems in either labelling or detecting croplands. For example, the moderate resolution of the ESACCI (300 m) and MCD12Q1 (500 m) products requires their classification schemes to use mosaic classes that mix cropland with other land-cover types. Such mosaic classes, which can underestimate cropland area[41] and therefore forest loss, nearly equalled or exceeded 'pure' cropland classes within these datasets over SEA (24% mosaic versus 15% pure in ESACCI; 5% versus 8% for MCD12Q1). For the higher-resolution GlobeLand30 (30 m), poor skill of its globally trained machine-learning algorithms in detecting irregularly shaped highland crop fields (for example, Fig. 1, Supplementary Figs. 5–14) could be the cause of its underestimation of highland forest loss (Fig. 4i).

Causes and impacts of cropland expansion in the highlands

The most striking result in our analyses is that these widely used land-cover-change products do not account for the rapid forest loss in SEA during the twenty-first century, particularly within highland regions of mainland SEA, where cropland expansion has been the key driver. This expansion has taken place despite an increase in protected forest areas (for example, national parks in Thailand, located primarily in highland areas, have increased from 96 in 1999 to 147 in 2015[42]) and the implementation of forest conservation policies (such as the prohibition on logging natural forests in Thailand since 1989[43]). This expansion also stands in marked contrast to the widespread agricultural retreat and forest recovery that has been occurring in other montane regions—for example, in the mountains of China where rural-to-urban migration and a series of government programmes have returned farmland to forest on sloping highlands[23]. Elsewhere, in Latin and Central America[44], the technology-induced intensification of agriculture has driven substantial deforestation in the lowlands; however, large-scale mechanized agriculture cannot be applied in highlands, allowing substantial forest recovery to take place[45].

In mainland SEA, however, market-driven intensification[38–40] has led to cropland expansion in the highlands[45]—such as conversions to corn (often for animal feed), coffee, tea, upland rice and other commodities in Thailand and Laos[6,7,29,39]. Pressure to expand cropping into these highland areas may be attributable to several reasons, including land scarcity. As of 2000, most of mainland SEA's lowlands were already utilized for some form of agriculture (in comparison, maritime SEA still had substantial areas of lowland forest remaining; Supplementary Fig. 15). National land-tenure policies and market pressures may have also increased local demands for new croplands in the highlands of mainland SEA[21,46]. Road developments may also have helped spur cropland development by increasing accessibility and facilitating transport of crops to markets[24,46,47]. Obtaining deeper insight into the causes of this rapid land-use change is important for anticipating the future trajectory of highland agriculture in mainland SEA, and determining whether it may eventually occur in maritime SEA, as its lowland forests become more supplanted by agriculture.

In general, we find a large amount of cropland-driven forest loss in SEA that has largely been ignored in both global assessments of land use and future projections. We estimate carbon emissions of 3,646 Mt due to forest loss in SEA during the early twenty-first century by integrating the satellite-based estimates of total carbon stored in trees[48] with our estimate of deforestation rate. These emissions are 103% higher than the estimate made by Pan et al.[14] using FAO Forest Resources Assessments, adding 14% (range: 7–123%) more carbon loss to global land-use-change emissions during the same period[1]. In addition, land-cover change in this region could have profound biophysical impacts on both the regional and global climate system that the current generation of climate simulations is missing because of the misrepresentations in their land-use products. The primary global atmospheric circulatory systems (for example, Hadley, Ferrel and polar cells) are strongly influenced by the intertropical convergence zone where the underlying surface receives strong solar heating. In Amazonia, for example, agricultural conversion of forests may result in regional warming of the land surface, cooling of the upper atmosphere and nearby oceans, and cause circulation changes that alter extratropical climates[2]. Incorporating the most accurate portrayal of SEA's highland land cover and potential future forest conversion into global climate models should be an immediate priority[1]. Finally, as tropical montane forests are hotspots of biodiversity because of their high endemism and diversity of threatened species, the possibility of future cropland-driven forest loss in highland SEA should warrant the attention of policymakers[6].

Methods

Methods, including statements of data availability and any associated accession codes and references, are available at https://doi.org/10.1038/s41561-018-0166-9.

Received: 18 January 2018; Accepted: 24 May 2018;
Published online: 02 July 2018

References

1. IPCC *Climate Change 2013: The Physical Science Basis* (eds Stocker, T. F. et al.) (Cambridge Univ. Press, 2013).
2. Feddema, J. et al. The importance of land-cover change in simulating future climates. *Science* **310**, 1674–1678 (2005).
3. Zeng, Z. et al. Climate mitigation from vegetation biophysical feedbacks during the past three decades. *Nat. Clim. Change* **7**, 432–436 (2017).
4. Zeng, Z. et al. Impact of Earth greening on the terrestrial water cycle. *J. Clim.* **31**, 2633–2650 (2018).
5. Alkama, R. & Cescatti, A. Biophysical climate impacts of recent changes in global forest cover. *Science* **351**, 600–604 (2016).
6. Crist, E. et al. The interaction of human population, food production, and biodiversity protection. *Science* **356**, 260–264 (2017).
7. Lawrence, D. & Vandecar, K. Effects of tropical deforestation on climate and agriculture. *Nat. Clim. Change* **5**, 27–36 (2015).
8. Wilcove, D. et al. Navjot's nightmare revisited: logging, agriculture, and biodiversity in Southeast Asia. *Trends Ecol. Evol.* **28**, 531–540 (2013).
9. Curran, L. et al. Lowland forest loss in protected areas of Indonesian Borneo. *Science* **303**, 1000–1003 (2004).
10. Margono, B. et al. Primary forest cover loss in Indonesia over 2000-2012. *Nat. Clim. Change* **4**, 730–735 (2014).
11. Achard, F. et al. Determination of deforestation rates of the world humid tropical forests. *Science* **297**, 999–1002 (2002).
12. Kim, D. et al. Accelerated deforestation in the humid tropics from the 1990s to the 2000s. *Geophys. Res. Lett.* **42**, 3495–3501 (2015).
13. Tomich, T., Thomas, D. & van Noordwijk, M. Environmental services and land use change in Southeast Asia: from recognition to regulation or reward? *Agric. Ecosyst. Environ.* **104**, 229–244 (2004).
14. Pan, Y. et al. A large and persistent carbon sink in the world's forests. *Science* **333**, 988–993 (2011).
15. Valentin, C. et al. Runoff and sediment losses from 27 upland catchments in Southeast Asia: impact of rapid land use changes and conservation practices. *Agric. Ecosyst. Environ.* **128**, 225–238 (2008).
16. Ahrends, A. et al. Current trends of rubber plantation expansion may threaten biodiversity and livelihoods. *Glob. Environ. Change* **34**, 48–58 (2015).
17. Hurni, K. et al. Mapping the expansion of boom crops in Mainland Southeast Asia using dense time stacks of Landsat data. *Remote Sens.* **9**, 320–346 (2017).
18. Fox, J. et al. Expansion of rubber mono-cropping and its implications for the resilience of ecosystems in the face of climate change in Montane Mainland Southeast Asia. *Glob. Environ. Change* **29**, 318–326 (2014).
19. Fox, F. et al. Simulating land-cover change in Montane Mainland Southeast Asia. *Environ. Manag.* **49**, 968–979 (2012).
20. Alexandratos, N. & Bruinsma, J. *World Agriculture Towards 2030/2050: The 2012 Revision* Working Paper No. 12-03 (FAO, 2012). .
21. Pongkijvorasin, S. & Teerasuwannajak, K. in *Sustainable Economic Development* (eds Balisacan, A. M. et al.) 105–122 (Academic Press, San Diego, 2015).
22. Kitchaicharoen, J. et al. *Situational Analysis in Support of The Development of Integrated Agricultural Systems in the Upland Areas of Nan Province* (Humidtropics, 2015).
23. Peng, W. et al. Research on soil quality change after returning farmland to forest on the loess sloping croplands. *J. Nat. Resour.* **20**, 272–278 (2005).
24. Cuo, L. et al. The roles of roads and agricultural land use in altering hydrological processes in Nam Mae Rim watershed, northern Thailand. *Hydrol. Process.* **22**, 4339–4354 (2008).
25. Pielke, R. & Avissar, R. Influence of landscape structure on local and regional climate. *Landsc. Ecol.* **4**, 133–155 (1990).
26. Wilson, A. & Barros, A. Orographic land–atmosphere interactions and the diurnal cycle of low-level clouds and fog. *J. Hydrometeorol.* **18**, 1513–1533 (2017).
27. Xue, Y. & Dirmeyer, P. Land-atmosphere interactions in monsoon regimes and future prospects for enhancing prediction. *CLIVAR Exch.* **19**, 28–32 (2015).
28. Hansen, M. et al. High-resolution global maps of 21st-century forest cover change. *Science* **342**, 850–853 (2013).
29. Stibig, H. et al. Change in tropical forest cover of Southeast Asia from 1990 to 2010. *Biogeosciences* **11**, 247–258 (2014).
30. Hansen, M. et al. Response to comment on "High-resolution global maps of 21st-century forest cover change". *Science* **344**, 981 (2014).

31. Olofsson, P. et al. Good practices for estimating area and assessing accuracy of land change. *Remote Sens. Environ.* **148**, 42–57 (2014).
32. Hurtt, G. et al. Harmonization of land-use scenarios for the period 1500–2100: 600 years of global gridded annual land-use transitions, wood harvest, and resulting secondary lands. *Climatic Change* **109**, 117–161 (2011).
33. Friedl, A. et al. *MODIS Collection 5 Global Land Cover: Algorithm Refinements and Characterization of New Datasets, 2001-2012* Collection 5.1 (Boston University, Boston, 2010); ftp://ftp.glcf.umd.edu/glcf/Global_LNDCVR/UMD_TILES
34. *Land Cover CCI: Product User Guide Version 2* (ESA, 2017); http://maps.elie.ucl.ac.be/CCI/viewer/download/ESACCI-LC-Ph2-PUGv2_2.0.pdf
35. Chen, J. et al. Global land cover mapping at 30 m resolution: a POK-based operational approach. *ISPRS J. Photogramm. Remote Sens.* **103**, 7–27 (2015).
36. Scott, J. *The Art of Not Being Governed: An Anarchist History of Upland Southeast Asia* (Yale Univ. Press, New Haven, 2014).
37. Stephen, S. Estimating area and map accuracy for stratified random sampling when the strata are different from the map classes. *Int. J. Remote Sens.* **35**, 4923–4939 (2014).
38. Bruun, T. et al. Environmental consequences of the demise in swidden cultivation in Southeast Asia: Carbon storage and soil quality. *Hum. Ecol.* **37**, 375–388 (2009).
39. Bruun, T. et al. Intensification of upland agriculture in Thailand: development or degradation? *Land Degrad. Dev.* **28**, 83–94 (2017).
40. Schmidt-Vogt, D. et al. An assessment of trends in the extent of swidden in Southeast Asia. *Hum. Ecol.* **37**, 269–280 (2009).
41. Ozdogan, M. & Woodcock, C. Resolution dependent errors in remote sensing of cultivated areas. *Remote Sens. Environ.* **103**, 203–217 (2006).
42. Suksawang, S. & McNeely, J. *Parks for Life: Why We Love Thailand's National Parks* (Clung Wicha, Nonthaburi, 2015).
43. Lakanavichian, S. in *Forest Out of Bounds: Impacts and Effectiveness of Logging Bans in Natural Forests in Asia-Pacific* (eds Durst, P. B. et al.) 167–184 (FAO, 2001).
44. Aide, T. et al. Deforestation and reforestation of Latin America and the Caribbean (2001–2010). *Biotropica* **45**, 262–271 (2013).
45. Byerlee, D. et al. Does intensification slow crop land expansion or encourage deforestation? *Glob. Food Secur.* **3**, 92–98 (2014).
46. Fox, J. & Vogler, J. Land-use and land-cover change in montane Mainland Southeast Asia. *Environ. Manage.* **36**, 394–403 (2005).
47. Sidle, R. & Ziegler, A. The dilemma of mountain roads. *Nat. Geosci.* **5**, 437–438 (2012).
48. Zarin, D. et al. Can carbon emissions from tropical deforestation drop by 50% in five years? *Glob. Change Biol.* **22**, 1336–1347 (2016).

Acknowledgements

This study was supported by Lamsam-Thailand Sustain Development (B0891). We thank Della Research Computing in Princeton University for providing computing resources. We thank CMIP for providing the IPCC global land-cover change forcing; J. Chen, D.-H. Kim and Hansen/UMD/Google/USGS/NASA for providing the moderate- and high-resolution satellite land-use/cover products; the Planet Lab and Google Earth for providing high-resolution satellite imagery; and the KASIKORN Foundation for data collection in the Nan province, Thailand. We also thank M. Pan and D. Gower for useful comments.

Author contributions

Z.Z. and E.F.W. designed the research. Z.Z. performed analysis. Z.Z., L.E. and A.D.Z. wrote the draft, and all authors contributed to the interpretation of the results and writing of the paper.

Competing interests

The authors declare no competing interests.

Additional information

Supplementary information is available for this paper at https://doi.org/10.1038/s41561-018-0166-9.

Reprints and permissions information is available at www.nature.com/reprints.

Correspondence and requests for materials should be addressed to Z.Z.

Publisher's note: Springer Nature remains neutral with regard to jurisdictional claims in published maps and institutional affiliations.

Methods

Satellite-observed high-resolution forest cover change in the twenty-first century. The freely available HANSEN product contains global maps of twenty-first-century forest cover change at a 30 metre spatial resolution (http://earthenginepartners.appspot.com/science-2013-global-forest). It is used widely for global forest monitoring by Global Forest Watch, as a part of World Resources Institute's Forest Frontiers Initiative (www.globalforestwatch.org). As described in Hansen and colleagues[28], the product developers used Google Earth Engine to analyse 654,178 Landsat 7 ETM+ images to characterize forest extent in 2000, forest gain during the period 2000–2012, forest loss during the period 2000–2014, and the year when forest loss occurred.

HANSEN product defines trees as all vegetation taller than 5 m in height. Furthermore, forest loss is defined as "a stand-replacement disturbance" (that is, the removal or mortality of trees), while forest gain is the establishment of tree "canopy from a non-forest state"[28]. These definitions take advantage of Earth observation images to capture the distribution of the biophysical features of Earth's surface[30]. Afforestation, including plantations of tree crops, is counted as forest gain. In this study, we avoid the areas afforested by focusing on the net forest loss pixels ($30\times30\,m^2$) where HANSEN product detected only forest loss but no gain during any year of the twenty-first century. We recognize the limitation of not being able to avoid the areas that were afforested recently, due to the lack of forest gain data since 2012 and the insufficient height of young plantations that are therefore not detected as forest gain. As these young tree plantations will ultimately grow to greater heights, we believe this limitation will be in part addressed by using forest gain data over a longer period (2000–2017, for example) using the next generation of HANSEN product (http://earthenginepartners.appspot.com/science-2013-global-forest).

The plausibility and accuracy of the HANSEN dataset. According to Hansen and colleagues[28], validation with FAO statistics, LiDAR detection and other satellite measurements show an overall accuracy higher than 99%, a user's accuracy of 87.0% and a producer's accuracy of 83.1% in the tropical domain[28]. In this study, we randomly selected 1,500 lowland and 2,500 highland sample pixels from NFLAs, and 500 lowland and 500 highland sample pixels from non-NFLAs (see Location columns in Supplementary Data 1–4). For each pixel, we applied Landsat 7 Enhanced Thematic Mapper Plus (ETM+) high-resolution satellite imagery scanned in 1999 (cloud-free) to interpret whether there was forest in the pixel before the twenty-first century (see the interpretation of high-resolution satellite imagery in 1999 columns in Supplementary Data 1–4). We also examined the land cover of our collection of 5,000 sample pixels in recent years by visual interpretations of high-resolution (≤5 m), cloudless satellite imagery (around or after 2014) available in the Planet Lab and Google Earth (see the interpretation of higher-resolution satellite imagery since 2014 columns in Supplementary Data 1–4; and the next section of the Methods). A pixel is labelled as NFLAs if there was forest in 1999 but not since 2014; otherwise, it is classified as non-NFLAs (for example, forest gain, stable forest and stable non-forest). In total, 93% of the pixels from NFLAs were accurately labelled as net forest loss, and 99% of the pixels from non-NFLAs as non-net forest loss. Spatially, the accuracy of the HANSEN product in the highlands is not greatly different from that in the lowlands (93% versus 94%; Supplementary Fig. 16). Most of the few incorrectly classified pixels occurred near the Equator (Supplementary Fig. 16), where the higher error is possibly due to more frequent cloud cover. Some of these misclassifications in mainland SEA's highlands might have been correct for their time period, but appeared incorrect in our assessment because of post-2014 changes that were captured in more recent high-resolution imagery. For example, swidden fields left fallow in 2013 could have appeared to be recovering forest in an image collected in 2017. Furthermore, it is possible that we misclassified some young tree crops as cropland in our visual interpretation of high-resolution (≤5 m) satellite imagery, owing to the following: (1) the seedlings were too small to be seen in the imagery, and (2) the intense cultivation practices on these lands (such as tillage, weeding, irrigation and/or fertilization) may appear similar to those on croplands. However, a previous image-interpretation-based cropland mapping effort has shown that young tree-crop plantations can be readily distinguished by human observers[49]. To test the effect of sample size on our assessment of HANSEN data accuracy, we recalculated the accuracy metrics after drawing random subsets of the data from 500 to 1,500 in lowland areas, and from 500 to 2,500 in highland areas. We found little change in the statistics (Supplementary Fig. 17), indicating that our assessment of HANSEN accuracy is unbiased by sample size.

Next, we undertook analyses of map accuracy and sample-based area estimation following Olofsson and colleagues[31]. The temporal reference sample (Supplementary Data 1–4) was applied to construct the error matrix of sample counts in SEA (Supplementary Table 3), highland SEA (Supplementary Table 4) and lowland SEA (Supplementary Table 5). The latter can be reformatted into the error matrix of estimated area proportions (Supplementary Tables 6–8) using the following equation:

$$p_{hj} = w_h \frac{n_{hj}}{n_h} \tag{1}$$

where p_{hj} is the sample-based estimated area proportion for map class h that belongs to reference class j, n_{hj} is the number of pixels in map class h that belongs to reference class j, w_h is the proportion of the total area in stratum (map class) h, and n_h is the total number of pixels in stratum h.

The error matrix of estimated area proportions (Supplementary Tables 6–8) was then used for the calculation of the overall, user's and producer's accuracies using equations (2–4):

$$O = \sum_{h=1}^{H} p_{hh} \tag{2}$$

$$U_h = \frac{p_{hh}}{p_h} \tag{3}$$

$$P_j = \frac{p_{jj}}{p_j} \tag{4}$$

where O is the overall accuracy, U_h is the user's accuracy for stratum h, P_j is the producer's accuracy for stratum j, p_h is the total area proportion in stratum h, and p_j is the total area proportion in stratum j.

The reference sample-based area for stratum j (A_{sj}) is estimated based on equation (5), and the 95% confidence interval of the estimated area for stratum j ($R_{sj}^{95\%}$) is calculated using equation (6).

$$A_{sj} = A_{mj} \sum_{h=1}^{H} p_{hj} \tag{5}$$

$$R_{sj}^{95\%} = 1.96 A_{mj} \sqrt{\sum_{h=1}^{H} \frac{w_h p_{hj} - p_{hj}^2}{n_h - 1}} \tag{6}$$

where A_{mj} is the map area for stratum j.

Using equations (2)–(6), the overall, user's and producer's accuracies of HANSEN-derived NFLAs are 98.4%, 93.2% and 81.2% in SEA; 98.4%, 92.8% and 71.6% in highland SEA; and 98.4%, 94.0% and 85.8% in lowland SEA. The net forest loss is 20.0×10^{10} m^2 (95% confidence interval: 19.8–20.3 $\times10^{10}$ m^2) in the lowlands, and 9.3 [9.1, 9.5] $\times10^{10}$ m^2 in the highlands. In total, the estimated area of net forest loss based on the reference is 29.3 [26.3, 32.3] $\times10^{10}$ m^2 in SEA.

In addition, we repeated the analysis with another 30 m resolution product from the Global Land Cover Facility (GLCF, www.landcover.org; ref. [12]), which was created using algorithms independent of HANSEN product (above; see also ref. [12]), and is part of NASA's MEaSURES project (Earth Science Data Records of Global Forest Cover Change). The GLCF product is composed of satellite-based maps of forest cover change in 34 countries spanning the humid tropics for years centred on 1990, 2000, 2005 and 2010[12]. A total of 5,444 Landsat scenes were collected from the Global Land Survey database to reproduce the tropical forest cover during the four epochs. Although the GLCF product has many missing values in maritime SEA due to extensive cloud cover (Supplementary Fig. 16), the cloud-free pixels show similar forest loss patterns as in the analysis using the HANSEN product (compare Supplementary Fig. 18 and Fig. 2a). In particular, widespread forest loss is also evident in the highlands of mainland SEA (Supplementary Fig. 18).

Post-disturbance land-cover analysis using very-high-resolution satellite imagery. To determine the fate of forest loss in NFLAs, we collected high-quality satellite imagery in recent years (around 2014; cloudless; of spatial resolution finer than 5 m) from the Planet Lab and Google Earth for all the 1,500 lowland and 2,500 highland pixels randomly selected from NFLAs. The sources of these high-resolution satellite imagery included two Google Earth products: (1) DigitalGlobe, which includes imagery from commercial satellites EarlyBird-1 (0.8–3.0 m), IKONOS (3.2 m), QuickBird (0.6–2.4 m), GeoEye-1 (0.41–1.65 m) and WorldView (0.25–1.84 m); and (2) CNES/Airbus, which includes the Pleiades-1A (0.5–2.0 m), Pleiades-1B (0.5–2.0 m), SPOT-6 and SPOT-7 (1.5–6.0 m) satellites. Two other products were provided by the Planet Lab (www.planet.com): (3) RapidEye (5 m); and (4) Doves (3 m; 4-band PlanetScope Scene).

In each pixel, we first checked for high-resolution (≤5 m), cloudless satellite imagery since 2014 in Google Earth (including DigitalGlobal and CNES/Airbus). If no images were present, we checked the RapidEye (5 m) satellite from the Planet Lab for the years between 2014 and 2016. Again, if no images were available, we checked the Doves (daily, 3 m) satellites from the Planet Lab for the period 2016 to 2017. We found qualified satellite imagery for all pixels (Supplementary Data 1 and 2), including 1,238 images from DigitalGlobal (193, 475, 375, 167 and 28 in 2014, 2015, 2016 and 2017, respectively), 1,169 images from CNES/Airbus (87, 643, 280, 101 and 58 in 2014, 2015, 2016 and 2017, respectively), 1,509 images from

RapidEye (1,363, 117 and 29 in 2014, 2015 and 2016, respectively) and 84 images from Doves (3 in 2016 and 81 in 2017).

We then used these randomly selected samples to examine whether the pixels ($30\times30\,m^2$) of NFLAs were covered by crops in recent years (around 2014; Supplementary Data 1 and 2, Fig. 3a). We estimated the percentage of forest loss into cropland in each 0.25° cell (δ_{crop}^{forest}, Fig. 3b) by extracting all the sampled pixels within the 3°×3° window centred on the cell and calculating the percentage of the pixels changing into cropland for that cell. On average, there are 73 samples in each moving window. However, some 3°×3° regions that experienced relatively little forest loss (for example, Southern Indonesia) received correspondingly fewer validation points (less than 10, in some cases); for these we expanded the moving window to 10°×10°. Collectively we found that δ_{crop}^{forest} approaches 100% in the lowlands, for both mainland and maritime SEA (Fig. 3b). In comparison, δ_{crop}^{forest} is lower in the highlands of SEA, particularly in western Myanmar, eastern Malaysia and northern Indonesia (Fig. 3b). Next, we mapped the spatial patterns of twenty-first-century cropland expansion in SEA (Fig. 3c) by multiplying the areas of forest loss with no gain (Fig. 2a) by δ_{crop}^{forest} (Fig. 3b) in each 0.25° cell. In the $29.3\times10^{10}\,m^2$ of areas where HANSEN product detected forest loss but no gain during the period 2000 to 2014, $27.0\times10^{10}\,m^2$ had been converted into cropland, including $8.2\times10^{10}\,m^2$ in highland regions, mostly in mainland SEA (Fig. 3c). The spatial pattern of cropland expansion ((loss − gain)×δ_{crop}^{forest}) and forest cover change (gain − loss) in SEA in the twenty-first century was mapped in Fig. 4a, showing that cropland expansion is not only driving forest loss in the lowlands of maritime SEA, but also the highlands of mainland SEA.

Global land-use/cover change products used for AR5 and AR6. We collected the land-use forcing data used in the Coupled Model Intercomparison Project Phase 5 (CMIP5) for IPCC AR5; ref. [1]) and that prepared for its next generation, IPCC AR6[32]. The products were generated with a global land-use model by the Land-Use Harmonization project, as a part of the Coupled Model Intercomparison Project under the World Climate Research Programme. The historical input datasets included population growth and land use (for example, cropland, pasture, urban and ice/water) based on the History Database of the Global Environment model[50] and the national wood harvest volume data from FAO statistics. In the climate change simulations for IPCC AR5, the historical runs were defined before 2005. Here we used land-cover change during the period 2000 to 2005 from the historical reconstructions, and that since 2006 from the four RCPs (RCP2.6, RCP4.5, RCP6.0 and RCP8.5). The land-use forcing for IPCC AR6 is constructed with updated inputs, and has a higher spatial resolution, more detailed land-use transitions and the addition of important agricultural management layers (Supplementary Data 3).

Land-cover reconstructions used in IPCC AR5[1], after 2005, followed assumed scenarios described by the RCPs, and thus suffer from deviations from the reality. Land-cover maps prepared for IPCC AR6[32] were reconstructed primarily based on FAO statistics. Statistical errors, if existing, can be introduced into this land-cover reconstruction. Because the FAO statistics were derived from national-scale data, land-cover information at smaller scales in LCMIP6 is model-derived, which is also an important source of uncertainty.

Satellite-based moderate- to high-resolution land-cover products. The Moderate Resolution Imaging Spectroradiometer (MODIS) Land Cover Type product (MCD12Q1; ref. [33]) was produced with a decision tree classification algorithm by integrating a database of high-quality land cover for training and the composited MODIS observations for forcing. MCD12Q1 supplied global maps of land cover at annual time steps and 500 m spatial resolution from 2001 to 2012. The product is composed of 17 types of land cover: water, evergreen needle-leaf forest, evergreen broad-leaf forest, deciduous needle-leaf forest, deciduous broad-leaf forest, mixed forest, closed shrublands, open shrublands, woody savannahs, savannahs, grasslands, permanent wetlands, croplands, urban and built-up, cropland/natural vegetation mosaic, permanent snow and ice and barren or sparsely vegetated areas. We focused on the changes in various types of forest and croplands. Here, evergreen needle-leaf forest, evergreen broad-leaf forest, deciduous needle-leaf forest, deciduous broad-leaf forest and mixed forest in MCD12Q1 were classified as a common forest land cover. Both croplands and cropland/natural vegetation mosaic in MCD12Q1 were classified as croplands. Cropland/natural vegetation mosaic accounts for 5% of all pixels throughout SEA in 2001, resulting in a large uncertainty in quantifying land-cover conversions between crop and other vegetation (mainly forest). The product is freely available at ftp://ftp.glcf.umd.edu/glcf/Global_LNDCVR/UMD_TILES.

The European Space Agency (ESA) Climate Change Initiative (CCI) provides moderate-resolution (300 m) global land-cover maps for three epochs centred on 2000, 2005 and 2010 (ESACCI; ref. [34]). This product was also produced with a machine-learning algorithm for land-cover classification. The product lists more than 22 types of land cover, including many mosaic types such as mosaic cropland (>50%)/natural vegetation (tree, shrub, herbaceous). In our study, all tree cover types, and mosaic tree and shrub, in ESACCI were classified as forest land. All crop cover types, and mosaic crop with other vegetation, in ESACCI were classified as croplands. Mosaic crop with other vegetation accounts for 24% of all pixels. The product is freely available at http://www.esa-landcover-cci.org/.

GlobeLand30 (ref. [35]) is the first open-access source of high-resolution maps of the Earth's land cover. It is the world's only global land-cover product at a 30 m resolution for the years 2000 and 2010. The GlobeLand30 was derived from more than 20,000 Landsat and Chinese HJ-1 satellite images based on the integration of pixel- and object-based methods using a machine-learning algorithm. There are no mosaic pixels in this classification scheme; and all pixels ($30\times30\,m^2$) were classified into cultivated land, forest, grassland, shrub land, wet land, water bodies, tundra, artificial surfaces, bare land and permanent snow and ice. The product is freely available at www.globeland30.org.

Data availability. Global land-use/land-cover change products used for IPCC AR5 are available at http://cmip-pcmdi.llnl.gov/cmip5/forcing.html#land-use_data; those for IPCC AR6 are available at http://luh.umd.edu/data.shtml. Satellite-based, moderate- to high-resolution land-cover products are available at ftp://ftp.glcf.umd.edu/glcf/Global_LNDCVR/UMD_TILES, http://www.esa-landcover-cci.org and http://www.globeland30.org. Satellite-observed high-resolution forest cover change in the twenty-first century is available at: http://earthenginepartners.appspot.com/science-2013-global-forest. All datasets are also available on request from Z.Z.

Code availability. The programs used to generate all the results were MATLAB (R2014a) and ArcGIS (10.4). Analysis scripts are available on request from Z.Z.

References

49. Estes, L. et al. A platform for crowdsourcing the creation of representative, accurate landcover maps. *Environ. Modell. Softw.* **80**, 41–53 (2016).
50. Chini, L., Hurtt, G. & Frolking, S. *Harmonized Global Land Use for Years 1500-2100* V1 (Oak Ridge National Laboratory Distributed Active Archive Center, 2014); https://doi.org/10.3334/ORNLDAAC/1248